Development of a 100 kW plasma torch for plasma assisted combustion of low heating value fuels

Sabri Takali, Frédéric Fabry, Vandad-Julien Rohani, François Cauneau, Laurent Fulcheri

Development of a 100 kW plasma torch for plasma assisted combustion of low heating value fuels

2014 J. Phys.: Conf. Ser. 550 012018

(http://iopscience.iop.org/1742-6596/550/1/012018)

Development of a 100 kW plasma torch for plasma assisted combustion of low heating value fuels

S Takali, F Fabry, V Rohani, F Cauneau and L Fulcheri[1]
MINES ParisTech, PSL-Research University, PERSEE Centre procédés, énergies renouvelables et systèmes énergétiques, CS 10207 rue Claude Daunesse 06904 Sophia Antipolis Cedex, France, Phone:+33.493.957.540.

E-mail: sabri.takali@mines-paristech.fr.

Abstract. Most thermal power plants need an auxiliary power source to (i) heat-up the boiler during start up phases before reaching autonomy power and (ii) sustain combustion at low load. This supplementary power is commonly provided with high LHV fossil fuel burners which increases operational expenses and disables the use of anti-pollutant filters. A Promising alternative is under development and consists in high temperature plasma assisted AC electro-burners. In this paper, the development of a new 100 kW three phase plasma torch with graphite electrodes is detailed. This plasma torch is working at atmospheric pressure with air as plasma gas and has three-phase power supply and working at 680 Hz. The nominal air flow rate is 60 $Nm^3.h^{-1}$ and the outlet gas temperature is above 2 500 K. At the beginning, graphite electrodes erosion by oxidizing medium was studied and controlling parameters were identified through parametric set of experiments and tuned for optimal electrodes life time. Then, a new 3-phase plasma torch design was modelled and simulated on ANSYS platform. The characteristics of the plasma flow and its interaction with the environing elements of the torch are detailed hereafter.

1. Introduction

The distribution of worldwide electrical power production shows that the main part of our electricity is produced by thermal power plants. Whether these plants are using fossil fuels or renewable combustibles, they all face start-up difficulties and the majority requires heavy fuel burner for several hours and consumes tons of high LHV fossil fuel to heat up the boilers and reach autonomy power. Some alternatives to these burners are actually under development. For instance, oxy-combustion [1], co-combustion [2] and plasma assisted combustion are three different alternatives[3][4][5]. The principal of the last alternative is mainly based on thermochemical activation of the combustion by thermal plasma (Figure 1). At chemical level, the plasma accelerates reaction kinetics and enhances the production of highly reactive radicals and ionised species such as atomic oxygen. At a thermal level, plasma torches can deliver high density of energy in a large volume of gas with a very high efficiency. Actually, the majority of thermal plasma torches is based on DC technology which suffers from reliability problems when operating with air, needs high maintenance costs and uses non consumable tungsten or copper electrodes. At centre PERSEE a new plasma torch is being developed based on years

[1] To whom any correspondence should be addressed

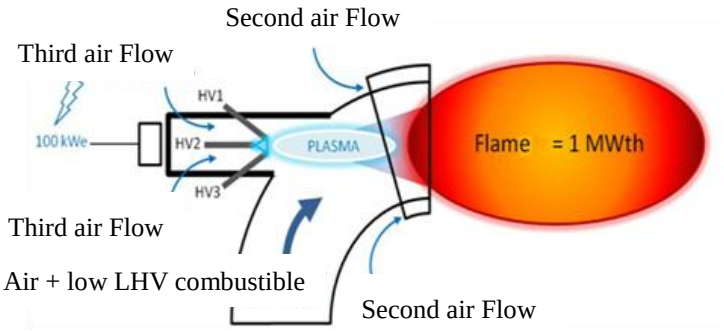

Figure 1. Schematic principle of Plasma electro-burner.

of know-how in the domain of three phase plasma torches for different application domains like syngas production or black carbon synthesis.

For the development of a more powerful three phase plasma torch working at atmospheric pressure with air and with graphite electrodes, preliminary tests are performed on previous generation of plasma torches to identify the main improvement axes. Actually, the existing plasma torches are mainly working with non-oxidizing gas such as hydrogen, nitrogen, CO, argon, helium or methane. So, the first step consists on studying the graphite electrodes erosion with air plasma gas in order to find the key parameters that can lead to erosion reduction. Furthermore, since we are aiming to increase the total power, arc discharge phenomena are also investigated in order to optimise the electro-thermal conversion efficiency at 100 kWe.

2. Preliminary study

2.1. Graphite electrode erosion

The first test campaign is conducted to evaluate the electrode erosion at different operating conditions: with non-oxidizing gas, with air or with a mixture of air and carbon black as plasma gas. The idea of injecting carbon powder with air consists in providing an alternative reactive medium for oxygen and protecting the graphite electrodes from oxygen. The test results are summarized in Table 1. These tests were performed at 200 A, the electric power reaches approximately 30 kW, with a total plasma gas flow rate of 5.6 Nm3.h-1. The first test is completed with nitrogen. If we neglect the formation of cyanide molecules (C-N) that occurs only at temperatures exceeding 3000 K [6], nitrogen can be considered as chemically neutral in presence of atomic carbon. Consequently, the eroded mass with nitrogen is low and mainly due to the electric discharge. In fact, under the effect of the temperature, the graphite sublimate at the cathode and anode spots [7]. Arc roots are also under the effect of ionic and electronic bombardment [8]. In presence of air, erosion by chemical reaction between oxygen and graphite is added to the previous erosion. Figure 2 shows the impact of both types of erosion: arc discharge effect is visible through impacts on the electrode tips with shape of craters and oxygen erosion is noticed on the lateral surface of each electrode.

The simulation of thermodynamic equilibrium of C, O2, and N2 mixtures between 273 K and 5000 K gives the proportions of all species that can coexist in the plasma zone as a function of the temperature. When oxygen is in excess, it reacts with all carbon atoms to form CO2 until 2000 K which dissociates then to atomic oxygen and CO. Yet, when carbon is more preponderate, it reacts with oxygen to produce CO2 until 700 K and then dissociates to give place to CO without residual atomic oxygen. It is this situation that we want to reproduce in the inter-electrode zone by injecting carbon powder at very small

granulometry in order to enhance CO formation and avoid the reaction between oxygen and graphite electrodes. Test results with CO as plasma gas show the pertinence of the idea. However, Table 1shows that contrarily to what is expected, increasing the C/O ratio leads to an increase of electrode erosion. A previous study of carbon black radiation in a plasma torch [9] shows that these particles behave like a thermal shield near the walls by absorbing the heat in the plasma zone leading to a decrease in wall heat losses. It is then possible that increasing the quantity of carbon particle for the same amount of energy, and for a very short residence time, concentrates more the energy in the discharge zone without reaching sublimation temperature to react with air. Consequently, the temperature rises and the impacts of air and discharge erosions are higher.

Table 1. Equivalent electrode life time in hours for a 0.12 m length and 0.017 m diameter electrode as a function of injected gas. The equivalent electrode life time is deduced from the equivalent eroded length calculated from the actual eroded mass as if the erosion takes place homogenously in the transversal section of the electrode.

Inlet plasma gas	Equivalent electrode life time in hours
Nitrogen	8.07
Air	2.80
Carbon monoxide	17.64
Mixture of air and solid carbon black (C/O=1)	2.81
Mixture of air and solid carbon black (C/O=1.15)	1.64
Mixture of air and solid carbon black (C/O=1.38)	1.60
Mixture of air and solid carbon black (C/O=1.75)	1.28

Figure 2. Top view of the discharge zone, the three graphite electrodes are in planar position.

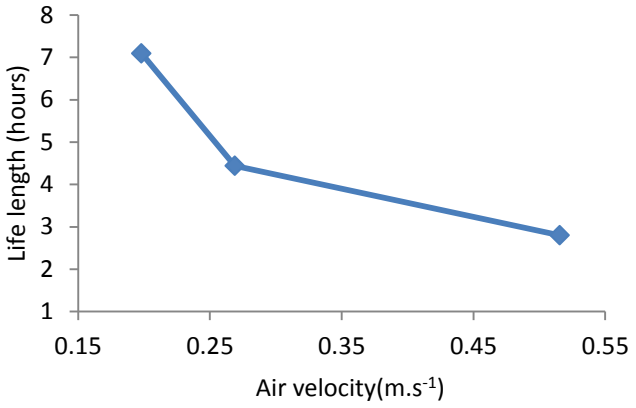

Figure 3. Graphite electrode life time as a function of air axial velocity at electrode tips in the planar three phase plasma torch geometry.

Another critical parameter for electrode erosion consists of air velocity impacting the lateral surface of the electrodes. In Figure 3 is plotted the electrode life time from different tests conducted at different air velocities in the inter-electrode zone. It can be noticed that by simply reducing the air flow velocity in this location, the electrode erosion decreases drastically. In addition, a minimum amount of nitrogen gas can be injected as protective layer around the electrode tips to prevent their erosion by air.

2.2. Power enhancement

In order to increase the electrical power of the new plasma torch design, the present study is based on the work of C. Rehmet [9] about electric arc behaviours in different geometries of three phase plasma torches. It is concluded that the impact of hydrodynamic electrode jet force is so significant that it changes the amount of power that could be provided by the arc for the same imposed current. For instance, in a planar electrode configuration, Lorentz force has a low impact on the arc column and the direction of the hydrodynamic electrode jets force -normal to the electrode tips- keeps the arc discharge confined in the inter-electrode gap (Figure 4). However, in an angular configuration, this hydrodynamic force is not directed toward the electrodes and the arc length increases (Figure 5). Besides, the interaction between the current lines in the arc column induces an increase of Lorentz force which leads to a global centrifugal arc motion. Consequently, the arc elongation due to the spatial position of the electrodes rises the arc column resistance and increases the electric discharge power for the same value of arc current. The choice of an electrode angle of 20° from the axis of the plasma torch is the result of these observations.

For technical reasons, mainly linked to plasma ignition and electrode gap, it is very difficult to have parallel electrodes although simulations show it is the best configuration for maximum arc power.

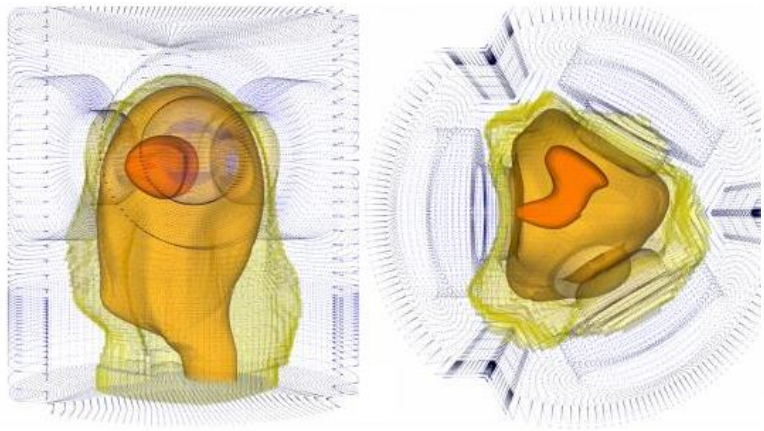

Figure 4. [Image courtesy of C. Rehmet]. Arc represented with temperature isosurfaces 15 000 K, 10 000 K and 5 000 K in coplanar electrodes configuration issued from MHD modelling.

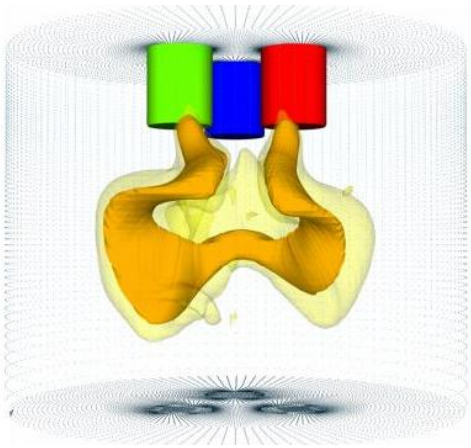

Figure 5. [Image courtesy of C. Rehmet].Arc discharge represented with temperature isosurfaces at 5 000 K and 8 000 K in parallel electrodes configuration issued from MHD modelling.

For better combustion assistance of the plasma, the gas at the outlet of the torch should reach a temperature high enough to provide radicals for the burner. A temperature range between 2 500 and 3 000 K is a compromise between the lower limit of oxygen dissociation and the upper limit of material resistance. For a 100 kWe plasma torch with a 70% thermal efficiency, the inlet flow rate needed to obtain a minimum of 2 500 K is about 0.02 kg.s-1 which gives an energy density of 1.11 kWh.Nm-3. In this case, the exhaust diameter has to be less than 0.15 m to obtain an outlet gas velocity of 10 m.s-1.

3. Simulation

3.1. Model, assumptions and boundary conditions

The objective of the modelling is to predict the plasma flow behaviour in regions where thermo-mechanical effects are preponderant (thermal and velocity fields), the quantification of heat losses through the walls and the validation of thermal reliability of the plasma torch components. In order to obtain coherent results yet inexpensive calculation cost, some assumptions are made and simplifications are suggested.

For simplification purposes only, one third of the plasma torch is modelled. This assumption is very rough since it implies neglecting the hydrodynamic force effect of the two opposite inlets but allows to considerably reduce the calculation cost. The second assumption consists on assuming that the plasma flow tends to a stationary state. However, the periodicity of the current and the nature of three phase plasma discharge -with all what it implies as electromagnetic and hydrodynamic forces- induce continuous perturbations. Yet, these forces are far of being periodic as shown in [10] and have some random aspects. Thus, adding the periodicity of the discharge to the simulation would not be a fair reproduction of the reality. In addition, the turbulence generated by these forces is located around the electric arc [10]. It is assumed that the unsteady phenomena due to the nature of three phase discharge are confined in a zone called the source volume. In the other hand, it is assumed that the local thermodynamic equilibrium (LTE) is verified which allows to define a unique temperature at each point of the plasma zone for all the species. The gas is considered incompressible i.e. apart from thermal dilatation effects, since the Mach number is considered always less than 0.3. The electromagnetic phenomenon is neglected here, since it is estimated that its effect is located in the power source volume.

The local balance equation for any intensive parameter g contained in a volume V with a delimiting surface S and containing the extensive parameter G could be expressed as; the variation of G inside V as a function of the time t is the sum of net entering flux of G through S and the creation of G inside V. With analytic terms this could be written as follows:

$$\frac{\partial \rho g}{\partial t} + \operatorname{div} \rho \vec{V} g + \operatorname{div} \overrightarrow{\varphi_{\mathrm{DG}}} - \rho g^{*} = 0 \qquad (1)$$

Where $\vec{V}$ and g^{*} are successively the velocity vector, the production term of g. Here, the flux is divided into convective and diffusive terms: $div\ \rho \vec{V} g, div\ \overrightarrow{\varphi_{DG}}$.

For mass balance, one should consider G as the mass and 1 for the intensive parameter g. Since there is no mass production, mass balance equation is directly:

$$\frac{\partial \rho}{\partial t} + \operatorname{div}\left(\rho \vec{V}\right) = 0 \qquad (2)$$

For the momentum balance equation, the velocity vector should be considered as the intensive parameter and the surface density of diffusive flux is equal to the stress tensor which could be written as: $\overrightarrow{\varphi_{DG}} = p\,\bar{\bar{I}} - \bar{\bar{\tau}}$ where p, $\bar{\bar{I}}$ and $\bar{\bar{\tau}}$ are successively the pressure, the unity tensor and the viscous stress tensor. The simplified equation becomes:

$$\rho \frac{\partial \vec{V}}{\partial t} + \operatorname{div} \rho \vec{V} \times \vec{V} + \overrightarrow{\operatorname{grad}}\, p - \overrightarrow{\operatorname{div}}\, \bar{\bar{\tau}} - \rho g^{*} = 0 \qquad (3)$$

To include turbulent phenomena in the simulation, the velocity is divided into average and fluctuating terms u_i. The k-ε turbulence model is the most common model used for plasma flow modelling [11], and adds two additional transport equations to equilibrate the additional two fluctuation parameters. The

transport variables are the turbulent kinetic energy k, and the turbulent dissipation ε. In the particular case of RNG k-ε model, these equations are as follows:

$$\frac{\partial(\rho k)}{\partial t}+\frac{\partial(\rho k u_i)}{\partial x_i}=\frac{\partial}{\partial x_j}\left(\alpha_k \mu_{eff}\frac{\partial k}{\partial x_j}\right)+\mathrm{G_k}+\mathrm{G_b}-\rho\varepsilon \tag{3.1}$$

$$\frac{\partial(\rho \varepsilon)}{\partial t}+\frac{\partial(\rho \varepsilon u_i)}{\partial x_i}=\frac{\partial}{\partial x_j}\left(\alpha_\varepsilon \mu_{eff}\frac{\partial \varepsilon}{\partial x_j}\right)+\mathrm{C_{1\varepsilon}}\frac{\varepsilon}{k}(\mathrm{G_k}+\mathrm{G_b})-\mathrm{C_{2\varepsilon}}\rho\frac{\varepsilon^2}{k}-R_\varepsilon \tag{3.2}$$

When replacing the intensive parameter with the gas enthalpy h we obtain the energy balance equation. The diffusion term consists of the heat flux by means of molecular conductivity which gives:

$$\frac{\partial \rho h}{\partial t}+\mathrm{div}\,\rho\vec{V}h+\mathrm{div}\left(\frac{\lambda}{C_p}\overrightarrow{\mathrm{grad}\,h}\right)-\rho g^*=0 \tag{4}$$

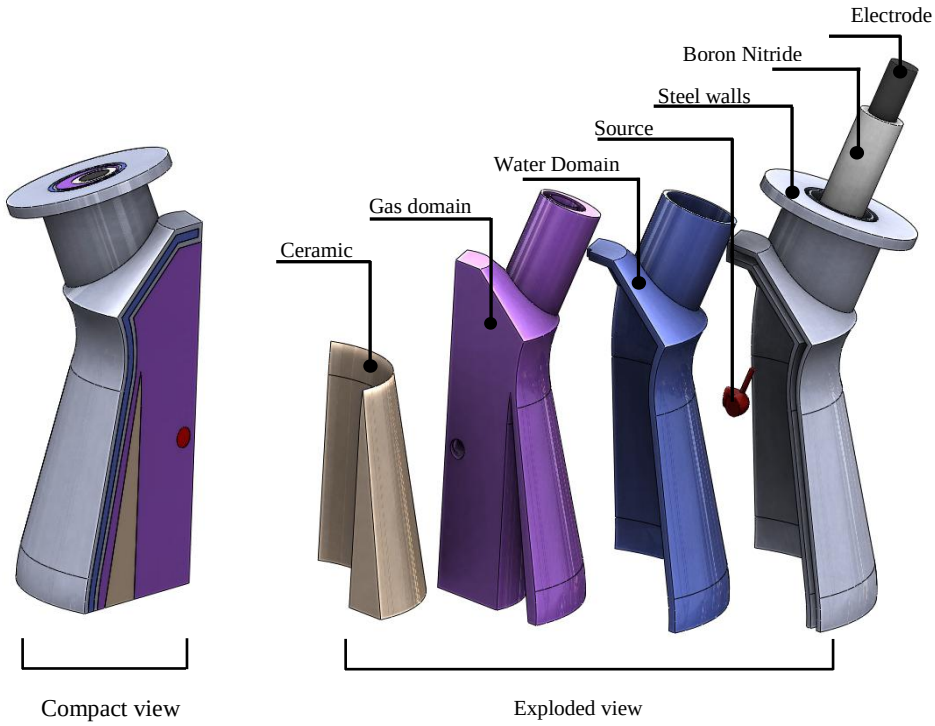

Figure 6. Compact and exploded views of the calculation domain.

These Navier-Stokes equations are the transport equation being solved numerically in Fluent. In this particular case, the integration of the water cooling circuit is necessary because the increase of the water temperature is a critical data at the laboratory scale were the external cooling system has a limited capacity for power extraction. Since the cooling system is part of the model, adjustment of the boundary conditions has minimal effect and is limited to outer walls where only convection heat transfer is considered, at a rate of 20 $W.k^{-1}.m^{-2}$ corresponding to forced air convection. Water inlet flow rate is at 0.27 $kg.s^{-1}$. For gas inlets, 18.33 $Nm^3.h^{-1}$ and 1.66 $Nm^3.h^{-1}$ are defined respectively for air and nitrogen inlet flow rates. The third of the power source contains 33.33 kW. These flow values coupled with the power injected and an exhaust diameter of 0.15m, give an estimation for the gas enthalpy of about 1.11

$kWh.Nm^{-3}$, an average temperature of around 2400 K for the outlet gas with an average velocity of around 7 $m.s^{-1}$.

The solid materials used for the model are stainless steel for the walls, ceramic for thermal sheeting, boron nitride for electric insulation and graphite for electrodes. Concerning air characteristics, the data used are defined up to 20 000 K and generated using TT-Winner software [6]. The geometry is edited and meshed using ANSYS geometry and meshing standard tools. Figure 6 show the different subdomains included in the simulation. For CPU consumption reason, the triangular meshing is enhanced with layer inflation at each interference and wall contact without predefined squeezed nodes. The maximum distance between nodes is set to 0.005 m and the total number of elements is 375000.

3.2. Simulation results

Figure 7 shows the gas expansion from the power source into the surrounding volume. The temperature inside the power source reaches almost 19 000 K according to the simulation, representing arc column and then decreases outsides with very high gradient to 1000 K in almost 0.03m. The gas accelerates inside the hot zone to a maximum of 50 $m.s^{-1}$ due to gas expansion. Nearby the power volume, we notice that the high energy content creates an important pressure gradient that aspires the air into the volume and forms vortices around the arc column. The ceramic element plays its role as a temperature shield and protects the steal walls from overheating by confining the gas expansion into the outlet and its maximum temperature is about 2000 K; 400 K less than its top operating limit. The heat losses to the walls are negligible and this is mainly due to the absence of radiation. This leads to higher outlet averaged temperature of about 4000 K. The electric insulation element is not also overheating although the proximity of the power source. The air layer passing between the ceramic and steel walls plays also its role in cooling the ceramic and avoiding the conduction of heat if they would be in contact. The current lines from the gas inlets show no backflow in the exhaust but some recirculation cells are created at the vicinity of the walls which may disturb arc discharge. The mass weighted average of molecular viscosity, density and velocity at the outlet are successively: 0.000115 $kg.m^{-1}.s^{-1}$, 12.2 $m.s^{-1}$ and 0.155 $kg.m^{-3}$, and knowing that the outlet diameter is 0.15 m, the Reynolds number is 2466. This means that the flow is not laminar and starts passing to turbulent state. At the frontier between cold and hot gas where the temperature gradient is high, Prandtl number reaches the value of 0.8 showing that thermal diffusion governed by the gas conduction and its specific heat capacity becomes as strong as the viscous diffusion characterized by the cinematic viscosity, whereas, inside and outside the plasma, thermal diffusion dominates. This means that this gas layer with high temperature gradient and high Prandtl number behaves more like a barrier that slows down the cold gas. The penetration of inlet air into the plasma is more occurring because of the depression. It is expected that hot and cold gas would not mix easily.

For graphite electrode erosion control, 5 $Nm^3.h^{-1}$ of nitrogen are injected between the electrodes and the electric insulation element surrounding the electrodes. In Figure 8, we see how the nitrogen is lowering the concentration of air in the inter-electrode zone which means less oxygen for electrode erosion. The nitrogen sheathing is more efficient near the torch axis. In fact, the torch is designed for lower velocity inside the discharge zone in order to prevent arc extinguishing. Figure 9, shows the temperature at different height levels. Above the arc column, we see how the air has higher velocity at the wall side of the electrode. The temperature is becoming more homogenous when moving down to the outlet. In Figure 10, the gas recirculation at the tip of the electrode shows how important is the shape of the source volume for a fair reproduction of the flow.

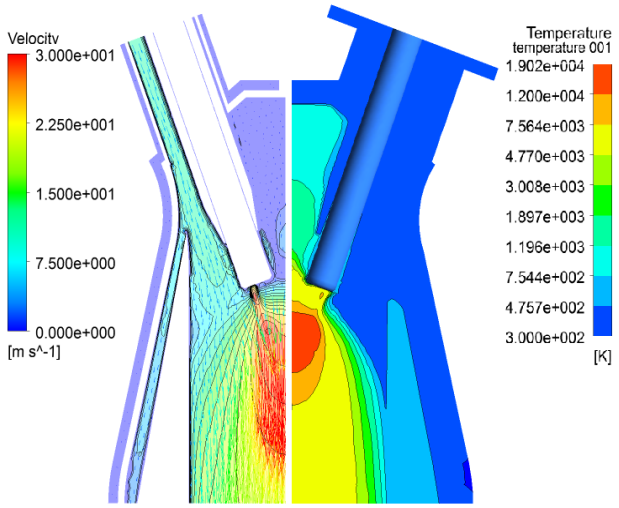

Figure 7. Velocity field (left), temperature field (right).

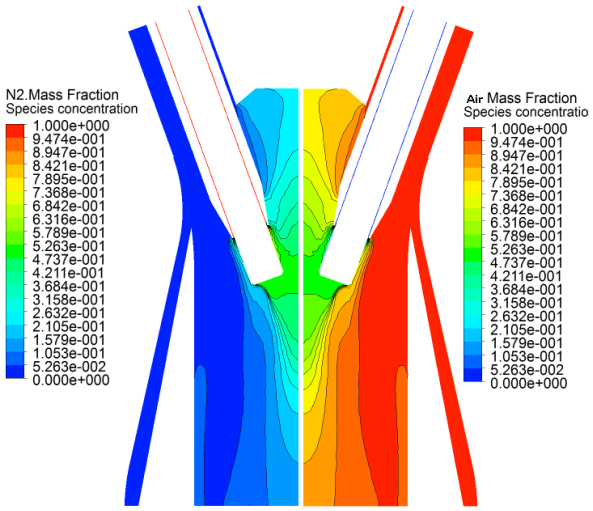

Figure 8. N2 mass fraction (left), Air mass fraction (right).

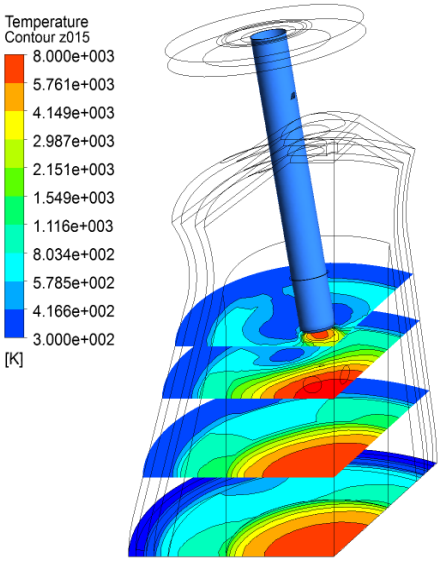

Figure 9. Temperature field at different level from the source volume (Temperature in the arc region exceeds 8 000 K).

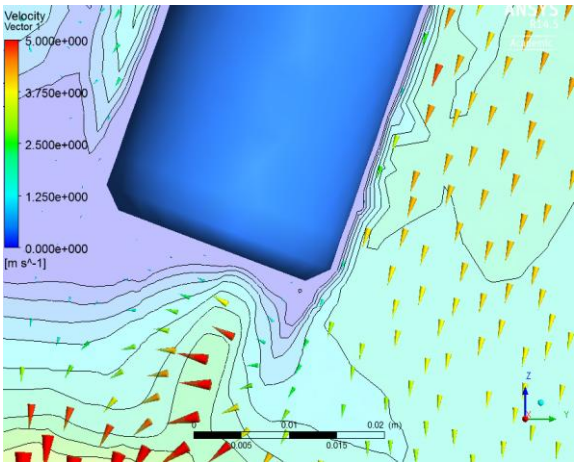

Figure 10. Velocity field around the electrode tip.

A parametric study is performed to investigate the effect of the power source volume on the plasma flow. Four different volumes are tested: 2 cm^3, 4 cm^3, 8 cm^3 and 16 cm^3. Figure 11 shows the gas temperature along radial position at different heights inside the torch: at 0.04m, 0.07m, 0.10 and 0.16m from the tip of the electrode. The mass averaged temperature of the power source volume are successively 17 011 K, 15 645 K, 14 538 K and 12 069 K starting from the smallest volume. Thus, when increasing the volume, the power density decreases and the mass averaged temperature decreases also. Nevertheless, the temperature outside the volume at z = 0.04 m is higher when the volume is bigger and

this is mainly due to the non-linearity of gas conductivity at high temperature. Besides, the volume change implies some differences in gas recirculation and thus the temperature field distribution is not exactly the same in the 4 cases as we see in Figure 12. These temperature variations become negligible at 0.06 m down to the source (0.10 m from the electrode tip) and the difference is also not noticeable above the source volume which means that for a global study of the plasma flow the source volume would not have big impact on the results.

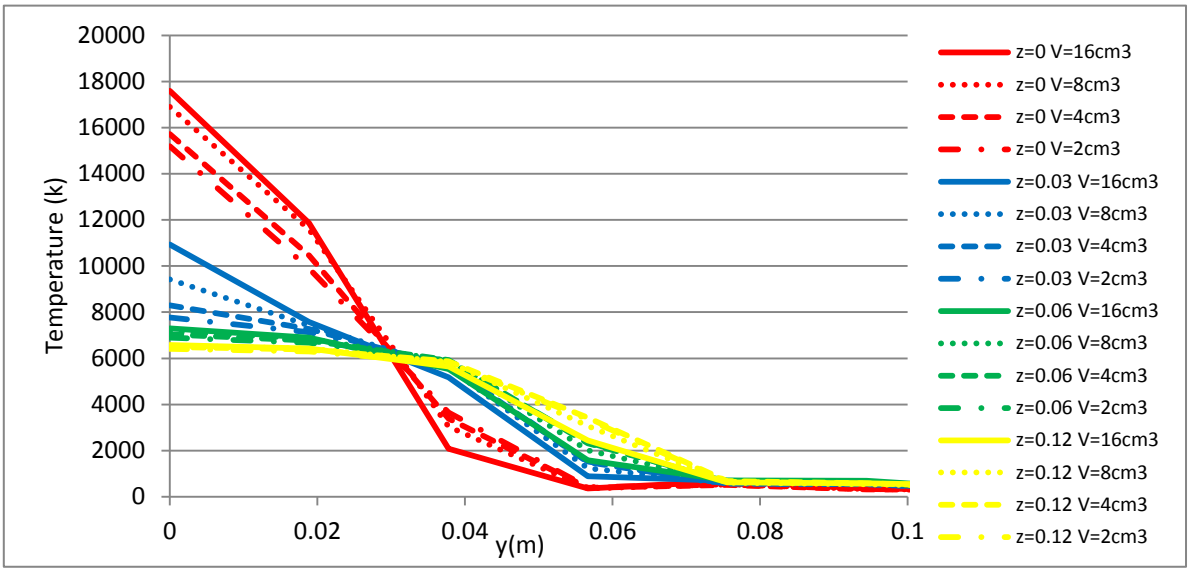

Figure 11. Gas temperature along the radial position (different source volume and vertical positions). (The plan defined by z = 0 is at 0.04m down to the electrode tips)

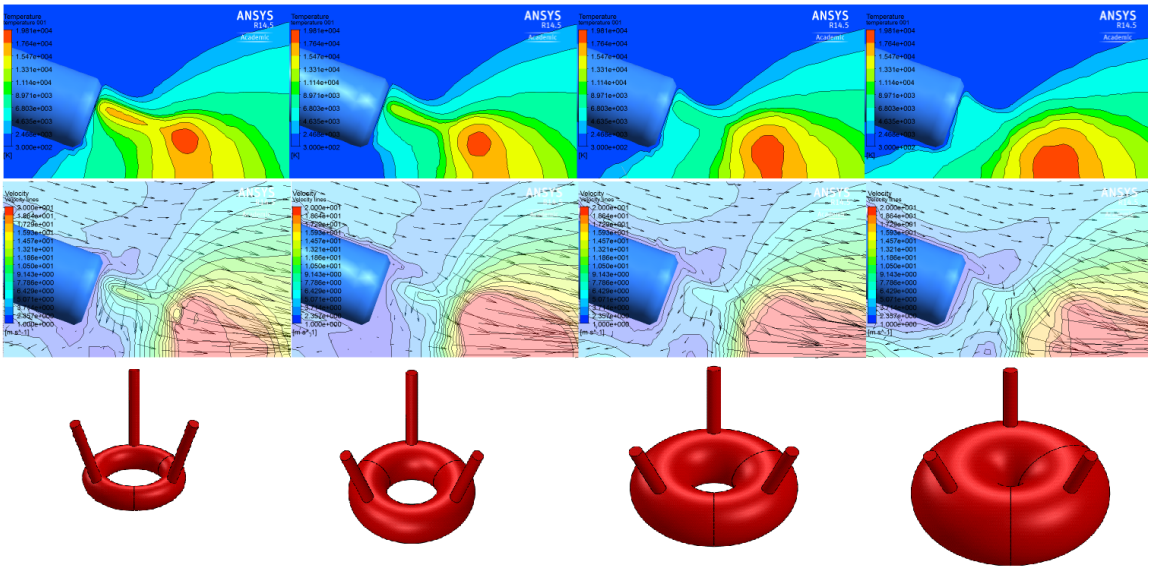

Figure 12. Temperature and velocity fields nearby the electrode tip (top) and arc column simplified shape (bottom) in 4 different volumes: 2 cm^3, 4 cm^3, 8 cm^3 and 16 cm^3.

The validation of the plasma flow and thermal behaviour of the different components of the 100 kW torch led to the manufacturing of the new torch which has been mounted on test bench and tested. The first start up test was successful and showed up to 80% heat efficiency. A series of test campaigns is

programmed for reliability validation and characterization of this torch. In addition, for better understanding of the plasma flow, more accurate simulations that take into account radiation will be performed.

4. Conclusion

The complexity of the graphite electrode erosion near the discharge zone in oxidizing atmosphere makes chemical control of the erosion very difficult and for this reason the aerodynamic control of air flow around the electrodes is kept as a solution by decreasing air speed at the tips. A shield of nitrogen is also injected around each electrode to provide a neutral boundary layer. The injection of methane could also be a solution for graphite erosion by depositing carbon atoms on the electrode surface. This alternative will be tested by replacing the nitrogen flow with methane. At the simulation level, we can deduce that, although the complexity of the phenomena taking place nearby the arc column, for global simulation it is possible to represent it with a source volume with the adequate shape.

5. References

[1] I. Pfaff and A. Kather, "Comparative thermodynamic analysis and integration issues of CCS steam power plants based on oxy-combustion with cryogenic or membrane based air separation," *Energy Procedia*, vol. **1**, no. 1, pp. 495–502, Feb. 2009.

[2] S. G. Sahu, N. Chakraborty, and P. Sarkar, "Coal–biomass co-combustion: An overview," *Renew. Sustain. Energy Rev.*, vol. **39**, pp. 575–586, Nov. 2014.

[3] M. A. GOROKHOVSKI, Z. JANKOSKI, F. C. LOCKWOOD, E. I. KARPENKO, V. E. MESSERLE, and A. B. USTIMENKO, "Enhancement of Pulverized Coal Combustion by Plasma Technology," *Combust. Sci. Technol.*, vol. **179**, no. 10, pp. 2065–2090, 2007.

[4] A. Askarova, E. . Karpenko, Y. . Lavrishcheva, V. E. Messerle, and A. Ustimenko, "Plasma-Supported Coal Combustion in Boiler Furnace," *IEEE Trans. Plasma Sci.*, vol. **35**, no. 6, pp. 1607–1616, Dec. 2007.

[5] T. Matsuura, K. Taniguchi, and T. Watanabe, "A new type of arc plasma reactor with 12-phase alternating current discharge for synthesis of carbon nanotubes," *Thin Solid Films*, vol. **515**, no. 9, pp. 4240–4246, Mar. 2007.

[6] G. D. Bernard PATEYRON, *T&Twinner, calculation and data bases of thermodynamics and transportation properties*. Direction des bibliothèques, des Musées et de l'Information Scientifique et technique, 1999.

[7] K. Katou, T. Asou, Y. Kurauchi, and R. Sameshima, "Melting municipal solid waste incineration residue by plasma melting furnace with a graphite electrode," *Thin Solid Films*, vol. **386**, no. 2, pp. 183–188, May 2001.

[8] Club E.D.F / Arc Electrique, Ed., *L'Arc électrique et ses applications*. Paris: Cnrs, 1984.

[9] C. Rehmet, V. Rohani, F. Cauneau, and L. Fulcheri, "3D Unsteady State MHD Modeling of a 3-Phase AC Hot Graphite Electrodes Plasma Torch," *Plasma Chem. Plasma Process.*, vol. **33**, no. 2, pp. 491–515, Apr. 2013.

[10] C. Rehmet, F. Fabry, V. Rohani, F. Cauneau, and L. Fulcheri, "High Speed Video Camera and Electrical Signal Analyses of Arcs Behavior in a 3-Phase AC Arc Plasma Torch," *Plasma Chem. Plasma Process.*, vol. **33**, no. 4, pp. 779–796, Aug. 2013.

[11] Q. Zhou, H. Li, X. Xu, F. Liu, S. Guo, X. Chang, W. Guo, and P. Xu, "Comparative study of turbulence models on highly constricted plasma cutting arc," *J. Phys. Appl. Phys.*, vol. **42**, no. 1, p. 015210, Jan. 2009.